

# Constraint on the stem cell numbers and division rates posed by the risk of cancer

Augusto Gonzalez<sup>1,2\*</sup>, Teresita Rodriguez<sup>3</sup>, and Rolando Perez<sup>1,3</sup>

<sup>1</sup>University of Electronic Science and Technology, Chengdu, People Republic of China

<sup>2</sup>Institute of Cybernetics, Mathematics and Physics, Calle E 309, Havana, CP 10400, Cuba

\*Corresponding author. Email: agonzale@icimaf.cu

<sup>3</sup>Center for Molecular Immunology, Havana, Cuba

## ABSTRACT

Compiled data for the stem cell numbers,  $N_s$ , and division rates,  $m_s$ , is reanalyzed in order to show that we can distinguish two groups of human tissues. In the first one, there is a relatively high fraction of maintenance (stem and transit) cells in the tissue, but the division rates are low. The second group, on the other hand, is characterized by very high transit cell division rates, of around one division per day. These groups do not have an embryonic origin. We argue that their properties arise from a combination of the needs of tissue homeostasis (in particular turnover rate) and a bound on cancer risk, which is roughly a linear function of the product  $N_s \times m_s$ . The bound on cancer risk leads to a threshold at  $m_s \approx 8/\text{year}$ , where the fraction of stem cells falls down two orders of magnitude.

## Cancer risk and the product $N_s \times m_s$ in a tissue

The purpose of the present paper is to show that the risk of cancer may pose a constraint on the number,  $N_s$ , and replication rate,  $m_s$ , of stem cells in a tissue. The starting point is a noticed correlation<sup>1,2</sup> between the risk and the product  $N_s \times m_s$ . To the best of our knowledge, the only explicit expression for the risk involving this product was obtained in a previous paper of ours<sup>3</sup>. For completeness, we briefly sketch the main steps leading to that expression.

A useful picture of normal and tumor tissues comes from processing gene expression (GE) data for small tissue samples<sup>4</sup>. A small sample is conformed by the contribution of many interacting cells, and is represented by a point in GE space, a tissue microstate. Recall, for example, the GE data provided by The Cancer Genome Atlas<sup>5</sup> for colon adenocarcinoma (COAD). A principal component (PC)<sup>6</sup> representation is shown in the top panel of Fig. 1. Two clouds of points are clearly distinguished. The normal samples are distributed around the origin of coordinates. The dispersion of points is related to regional differences and the fact that the samples come from different patients. An ellipse representing the r.m.s. radii along each axis is drawn. The tumor samples, on the other hand, are far apart along the PC1 axis. An ellipse with the r.m.s. cloud radii is also drawn. Let us denote by  $\bar{x}_1$ ,  $R_n$ , and  $R_t$  the position along PC1 of the center of the tumor cloud, and the r.m.s. radii along PC1 of the normal and tumor clouds, respectively. It is apparent that the distance between cloud centers,  $\bar{x}_1 = 155.89$ , is much larger than any of the radii  $R_n = 11.71$  or  $R_t = 28.53$ .

Both the normal and tumor regions may be qualified as attractors in GE space<sup>7</sup>. they may sustain long time oscillations of microstates. Their radii  $R_n$  and  $R_t$  define their basins of attraction.

Normal and tumor attractors could be understood as global stable solutions of GE networks<sup>8</sup>. We prefer, however, to interpret them as local maxima in the fitness landscape. The center panel of Fig. 1 contains a sketch of the fitness along the PC1 axis. The y axis is the fitness with a minus sign. The centers

of the clouds correspond to local maxima. We computed the volumes of the basins of attraction, which provide an estimation of the number of available microstates<sup>9</sup>. This number is much higher for tumors than for normal samples. In addition, the replication rates of tumor stem cells is usually larger than the rate of normal cells<sup>10</sup>. The conclusion is that the tumor minimum is the deepest in Fig. 1 central panel, i.e. the one with the highest fitness. The intermediate region,  $R_n < x_1 < \bar{x}_1 - R_t$ , correspond to a low fitness barrier separating the wells. The scarcity of samples in this region is an evidence of the low fitness values. The barrier is needed in order to prevent the spontaneous transitions from the normal to the tumor regions, driven by the fitness difference.

The PC1 axis describes progression to cancer. A normal sample evolving to a tumor state realizes a motion along the PC1 axis from a point near the origin to a point near  $\bar{x}_1$ . We have schematically drawn its motion in the bottom panel of Fig. 1.

The random displacements, i.e. random variations in the GE of a gene or a group of genes, are caused by spontaneous somatic mutations<sup>11</sup>, epigenetic changes<sup>12</sup> or the action of external factors<sup>13</sup>. Because the normal region is a local maximum of fitness, the sample may experience random displacements, but remain in the normal region for a long time. Only when the random displacements drive the sample out of the normal region it may experience a drift towards the tumor zone. Notice that the distance between normal and tumor regions is  $R = \bar{x}_1 - R_n - R_t$ . This is the minimal length of a path connecting both regions.

Among the random motions in GE space, we distinguish small (Brownian) displacements and large (Levy) jumps. The former are most likely caused by independent gene variations, whereas the latter represent the coordinated variations of a set of genes. Levy jumps are described by power-like distribution functions, which are very common in mutations<sup>14</sup>, and in the GE distribution functions of eukaryotes<sup>15,16</sup>. The Levy jumps could perhaps be identified as the hits in the multistep theory of cancer<sup>17</sup>.

In the bottom panel of Fig. 1, a trajectory which combines Brownian motions and large jumps is drawn. However, the parameters (fluctuation scale and the rate of large jumps) have been exaggerated in order to make the effects apparent.

Under the assumption that Levy jumps are rare (unfrequent) events, we compute the one-hit probability to transit from the normal to the tumor region, leading to the following expression for the risk<sup>3</sup>:

$$\frac{risk}{N_s} = \mu \frac{D}{R} (t_0 + m_s \times age). \quad (1)$$

The parameter  $D$  sets the scale for fluctuations.  $\mu$  is the effective rate of large jumps. In an effective way, it accounts for the effects of hereditary factors, external carcinogens, the role of the immune system, etc.  $t_0 = \log_2 N_s$ . For the set of tissues considered in Refs.<sup>1,2</sup>,  $t_0$  is a number around 30. On the other hand,  $m_s \times age$  is the number of stem cell generations measured from the time  $t_0$  at which the tissue is formed. For many tissues, the product  $m_s \times age$  is larger than 30, thus appart from nearly constant magnitudes,  $risk \sim N_s \times m_s$ .

The analysis in the next section is based on Eq. (1), or its simpler version  $risk \sim N_s \times m_s$ .

## Results

### Groups of tissues and risk of cancer

Table 1 contains a summary of the compiled data<sup>1,2</sup>. The data shows relatively large variations. For example, the stem-cell division rate in colon crypts is reported by the authors to be 73/year, whereas for bronchio-alveolar cells the rate is around 0.07/year, i.e. three orders of magnitude smaller. Similar

variations are exhibited by the number of stem cells or the quotient  $N_s/N_{cell}$  between the stem and total cell numbers in the tissues.

In Fig. 2, upper panel, we represent tissues as points in the  $(m_s, N_s)$  plane. Because of Eq. (1), tissues with similar risks of cancer should be located roughly along a hyperbola with a given value of the product  $N_s \times m_s$ . If there is a maximal allowed risk, then the corresponding hyperbola would divide the quadrant in allowed and forbidden regions. An increase of the division rate should be compensated by a decrease in the stem cell number, and viceversa, in order to keep the risk below the maximum. Thus, we can distinguish tissues with relatively “high division rates” (and low stem cell numbers) or “high stem cell numbers” (and low division rates).

In Fig. 2, lower panel, logarithmic scales are used in order to make apparent the groups of tissues. First, we have the undifferentiated cells (melanocytes, ovarian germ cells), represented by diamonds, for which  $N_s/N_{cell} = 1$ . Next, there is a group we call Type I tissues (circles), characterized by a relatively high fraction of stem cells and division rates lower than around 8/year. They correspond mainly to interior organs, although the epidermis also belongs to this group. Finally, we have Type II tissues (squares) with relatively high division rates,  $m_s \geq 8/\text{year}$ , and low fractions of stem cells.

This lower panel shows that each group (I and II) exhibits a monotonous dependence of  $N_s$  on  $m_s$ . In the next subsection, we argue that this is indeed a parametric dependence. Different tissues inside a group differ in the average replacement rate of their differentiated cells. As this parameter is increased, both  $N_s$  and  $m_s$  increase, leading to the observed monotony.

The enigmatic threshold at  $m_s \approx 8/\text{year}$  separating the two groups, where the fraction of stem cells falls down two orders of magnitude, could be understood in terms of a maximal allowed risk of cancer dictated by evolution. A tissue in Group I could not go beyond the extremal point (the skin, which defines the extremal hyperbola), thus a tissue with a higher average replication rate could be realized only as a Group II tissue.

Notice, for example, that the risk of cancer in the male germinal cells, first point in the lower curve, is reduced by two orders of magnitude as compared to the risk in the skin, which has a similar value of  $m_s$ .

The maximal allowed value for the risk could be estimated as half the observed risk for basal cell carcinoma. Indeed, the reported value of 0.3<sup>1</sup>, corresponds to an age equal to 80 years. The biological age for our species is, however, only around 40 years<sup>18</sup>, thus according to Eq. (1), the maximal allowed risk in human tissues should be around 0.15.

## Tissue groups and homeostasis

In this subsection, we consider the tissue under stationary conditions, i.e. homeostasis, and examine the equations determining the number of cells. We shall see that these equations offer another point of view to the origin of the group of tissues mentioned above.

We assume that, in addition to stem, in the tissue there are a number  $N_t$  of transit amplifying cells, and a number  $N_d$  of fully differentiated cells. We schematically represent in Fig. 3 the equilibrium equations. The diameters of circles in the figure indicate that  $N_d \gg N_t \gg N_s$ . Arrows represent rates of division ( $m_s, m_t$ ), differentiation ( $r_s, r_t$ ) or replacement ( $r_d$ ).

Under homeostatic conditions, the number of cells are nearly constant, meaning that fluxes should be equilibrated:

$$\begin{aligned} m_s N_s &= r_s N_s, \\ r_s N_s + m_t N_t &= r_t N_t, \\ r_t N_t &= r_d N_d. \end{aligned} \tag{2}$$

The first equation leads to  $m_s = r_s$ . The next two may be rewritten as:

$$\begin{aligned} r_t - m_t &= \frac{N_s}{N_t} m_s \ll m_s, \\ r_t &= \frac{N_d}{N_t} r_d \gg r_d. \end{aligned} \quad (3)$$

In addition, it is expected that the division rate of transit cells is much higher than that of stem cells, thus  $r_t$  and  $m_t$  are very close and we arrive to the conditions:  $m_t \approx r_t \gg m_s$ , and  $m_t \gg r_d$ .

The above equations may help understanding the groups apparent in Fig. 2 lower panel. Inside a group, we expect an increase of  $m_s$  when  $r_d$  is increased. This does not follow from the equations, but is a very plausible hypothesis. With regard to the fraction of stem cells, we may write an equation for  $N_s/N_d$ :

$$\frac{N_s}{N_d} = \frac{r_d}{m_s} (1 - m_t/r_t). \quad (4)$$

As mentioned. the left hand side of the equation should be less than one. The difference between the two groups comes from the expression in parenthesis. In the second group of tissues this expression takes a value much closer to zero, because  $m_t$  and  $r_t$  simultaneously take very large values, and their ratio is very close to one.

We may examine some of the studied tissues in quality of examples. Let us start with the epidermis, the one with the highest division rate in Type I tissues, with  $m_s = 7.6/\text{year}$ . Authors of Ref.<sup>1</sup> provide the following estimations:  $N_s/N_{cell} \approx 0.032$ ,  $N_t/N_{cell} \approx 0.29$ , from which it follows that  $(N_t + N_s)/N_{cell} \approx 0.32$ . This high proportion of maintenance cells seems to be the distinctive characteristic of Type I tissues. From these numbers and the replacement rate  $r_d \approx 18/\text{year}$ <sup>19-21</sup>, we get  $r_t \approx 42/\text{year}$  and  $m_t \approx 41/\text{year}$ .

On the other hand, let us consider the Type II tissue with the highest division rate: the colon. Because of the derived relation,  $m_t \gg m_s \approx 73/\text{yr}$ , we expect  $m_t$  to be around 200/year or even higher. Notice that there is a characteristic value for the division rate of fast replicating human tissues<sup>23</sup>, of around one division per day or 400/yr.

In order to verify that this characteristic, a high  $m_t$  close a circadian variation, is distinctive of Type II tissues, we examine blood, which is in the opposite “low- $m_s$ ” side. Blood, with  $m_s \approx 12/\text{year}$ , exhibits a complex pattern of differentiation channels. The replacement rate of neutrophils, for example, is  $r_d \approx 73 - 365/\text{year}$ <sup>19,22</sup>. Because of the condition  $m_t \gg r_d$ , we get again a very high value for  $m_t$  in the neutrophil line.

## Concluding remarks

According to data provided by papers<sup>1,2</sup>, and their suggestion that the product  $N_s \times m_s$  (multiplied by the age) is an indicator of the risk of cancer in the tissue, further supported by Eq. (1), we suggest a classification of tissues dictated by their position in the  $(m_s, N_s)$  plane.

Type I, i.e. “high- $N_s$ , low- $m_s$ ”, tissues are characterized by a high proportion of maintenance cells, reaching one third. Type II, i.e. “high- $m_s$ , low- $N_s$ ” tissues, on the other hand, exhibit very high values for the division rates of transit amplifying cells, reaching 400 divisions per year.

Each group of tissues conform a well defined cluster, as shown in Fig. 2 lower panel. The equations determining the numbers of cells in a tissue under homeostatic conditions allow a qualitative understanding of the two groups in terms of the fraction of stem to total number of cells and the division rate of transit

amplifying cells. The threshold value  $m_s \approx 8/\text{year}$ , separating the two groups, could be dictated by an upper bound imposed on the risk by evolution, and the possibility of a second solution of the master equations determining the number of cells.

## Acknowledgements

A.G. acknowledges the Cuban Program for Basic Sciences, the Office of External Activities of the Abdus Salam Centre for Theoretical Physics, and the University of Electronic Science and Technology of China for support. The research is carried on under a project of the Platform for Bioinformatics of BioCubaFarma, Cuba.

## Author contributions statement

A.G. is responsible for the analysis based on master equations and redaction of an initial draft. All authors analyzed the data and reviewed the final version of the manuscript.

## Additional information

**Competing interests** The authors declare that there are not competing interests.

## References

1. C. Tomasetti and B. Vogelstein, Variation in cancer risk among tissues can be explained by the number of stem cell divisions, *Science* 347, 78-81 (2015).
2. Cristian Tomasetti, Lu Li and Bert Vogelstein, Stem cell divisions, somatic mutations, cancer etiology, and cancer prevention, *Science* 355 (2017) 1330-1334.
3. Roberto Herrero, Dario Leon and Augusto Gonzalez (2020). Levy model of cancer. arXiv:1507.08232 (unpublished).
4. Augusto Gonzalez, Yasser Perera and Rolando Perez (2020). On the gene expression landscape of cancer. arXiv:2003.07828 (unpublished).
5. The TCGA Research Network: <https://www.cancer.gov/tcga>. Accessed Sept. 2019.
6. Jake Lever, Martin Krzywinski and Naomi Altman (2017). Principal component analysis. *NATURE METHODS* 14: 641-642.
7. Sui Huang, Ingemar Ernberg, and Stuart Kauffman (2009). Cancer attractors: A systems view of tumors from a gene network dynamics and developmental perspective. *Semin. Cell. Dev. Biol.* 20(7): 869–876.
8. Frank Emmert-Streib, Matthias Dehmer and Benjamin Haibe-Kains (2014). Gene regulatory networks and their applications: understanding biological and medical problems in terms of networks. *Frontiers in Cell and Developmental Biology* 2: 38.
9. Frank Quintela and Augusto Gonzalez (2020). Estimating the number of available states for normal and tumor tissues in gene expression space. arXiv:2005.02271 (unpublished).
10. Sten Friberg and Stefan Mattson, On the Growth Rates of Human Malignant Tumors: Implications for Medical Decision Making, *Journal of Surgical Oncology* 65 (1997) 284-297.

11. Iñigo Martincorena and Peter J. Campbell (2015). Somatic mutation in cancer and normal cells. *Science* 349(6255): 1483-1489.
12. Keith D. Robertson (2005). DNA methylation and human disease. *Nature Reviews Genetics* 6: 507.
13. J.L. Barnes, M. Zubair, K. John, et. al. (2018). Carcinogens and dna damage. *Biochem. Soc. Trans.* 46 (5): 1213–1224.
14. Dario Leon and Augusto Gonzalez (2020). Mutations as Levy flights. arXiv:1605.09697 (unpublished).
15. V. A. Kuznetsov, G. D. Knott and R. F. Bonner (2002). General Statistics of Stochastic Process of Gene Expression in Eukaryotic Cells. *Genetics* 161: 1321–1332.
16. Augusto Gonzalez, Joan Nieves, Maria Luisa Bringas, Pedro Valdes-Sosa (2020). Gene expression rearrangements denoting changes in the biological state. arxiv:1706.09813 (unpublished).
17. Steven A. Frank (2007). Dynamics of cancer: incidence, inheritance and evolution. Princeton University Press. New Jersey.
18. Michael Gurven and Hillard Kaplan (2007), Longevity among hunter-gatherers: a cross-cultural examination. *Population and Development Review* 33(2): 321–365.
19. Harvard bionumbers database. <https://bionumbers.hms.harvard.edu>.
20. G.D. Weinstein, E.J. Van Scott (1965)). Autoradiographic analysis of turnover times of normal and psoriatic epidermis. *J. Invest. Dermatol.* 45(4): 257-262.
21. S. Rothberg, R.G. Crouse, J.L. Lee (1961). Glycine-C-14-incorporation into the proteins of normal stratum corneum and the abnormal stratum corneum of psoriasis. *J. Invest. Dermatol.* 37: 497-505.
22. Rainer Flindt (2006). Amazing numbers in biology. Springer-Verlag, Berlin.
23. S. Bernard, H. Herzel (2006). Why do cells cycle with a 24 hour period?. *Genome Inform.* 17(1):72-79.

Undifferentiated cells	$N_{cell}$	$N_s$	$m_s$ (1/yr)
Melanocytes	$3.8 \times 10^9$	$3.8 \times 10^9$	2.48
Ovarian germinal cells	$1.1 \times 10^7$	$1.1 \times 10^7$	< 0.012
Type I tissues	$N_{cell}$	$N_s$	$m_s$ (1/yr)
Epidermis	$1.8 \times 10^{11}$	$5.82 \times 10^9$	7.6
Breast	$6.8 \times 10^{11}$	$6.5 \times 10^9$	4.3
Prostate	$3 \times 10^{10}$	$2.1 \times 10^8$	3
Pancreas	$1.97 \times 10^{11}$	$4.92 \times 10^9$	1
Hepatocytes	$2.41 \times 10^{11}$	$3.01 \times 10^9$	0.9125
Gallbladder	$1.6 \times 10^8$	$1.6 \times 10^6$	0.584
Thyroid	$1.1 \times 10^{10}$	$8.25 \times 10^7$	0.087
Bronchio alveolar cells	$4.34 \times 10^{11}$	$1.22 \times 10^9$	0.07
Bone cells	$1.9 \times 10^9$	$4.18 \times 10^6$	0.067
Cerebellum	$8.5 \times 10^{10}$	$1.36 \times 10^8$	< 0.012
Brain	$1.707 \times 10^{11}$	$2.73 \times 10^8$	< 0.012
Type II tissues	$N_{cell}$	$N_s$	$m_s$ (1/yr)
Colon	$3 \times 10^{10}$	$2 \times 10^8$	73
Small Intestine	$1.7 \times 10^{10}$	$1 \times 10^8$	36
Esophagus	$3.24 \times 10^9$	$6.65 \times 10^6$	33.18
Head and Neck	$1.67 \times 10^{10}$	$1.85 \times 10^7$	21.5
Blood cells	$3 \times 10^{12}$	$1.35 \times 10^8$	12
Germ cells Testis	$2.16 \times 10^{10}$	$7.2 \times 10^6$	5.8

**Table 1.** Data, coming from Refs. <sup>1,2</sup>, for different human tissues.

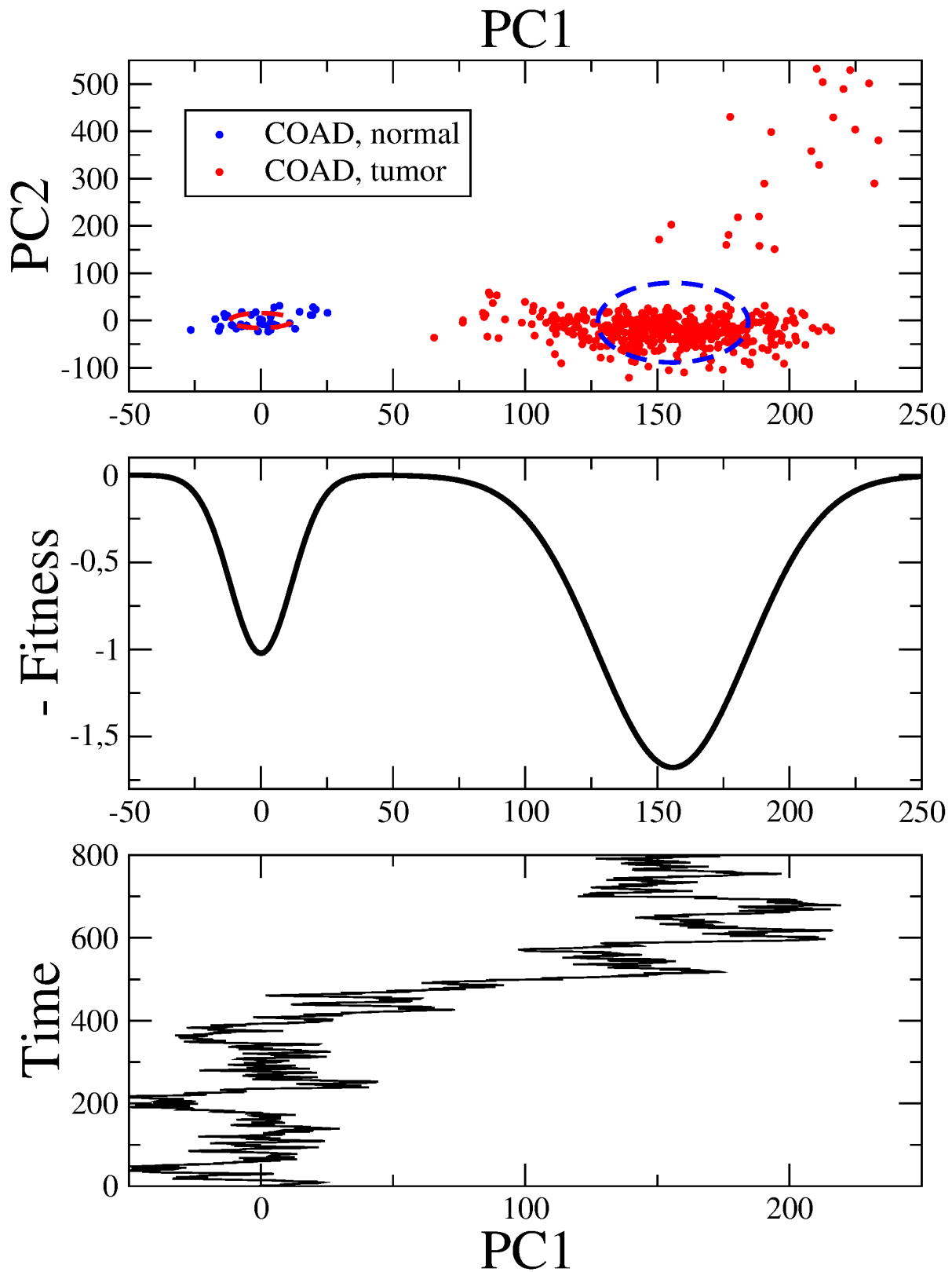


**Figure 1.** Top: A PCA representation of the GE data in COAD. Ellipses illustrate the magnitudes of the r.m.s. radii along each direction. Center: Schematic representation of fitness along the PC1 axis. Bottom: Time evolution of a microstate which starts in the normal region and transits to the tumor region.



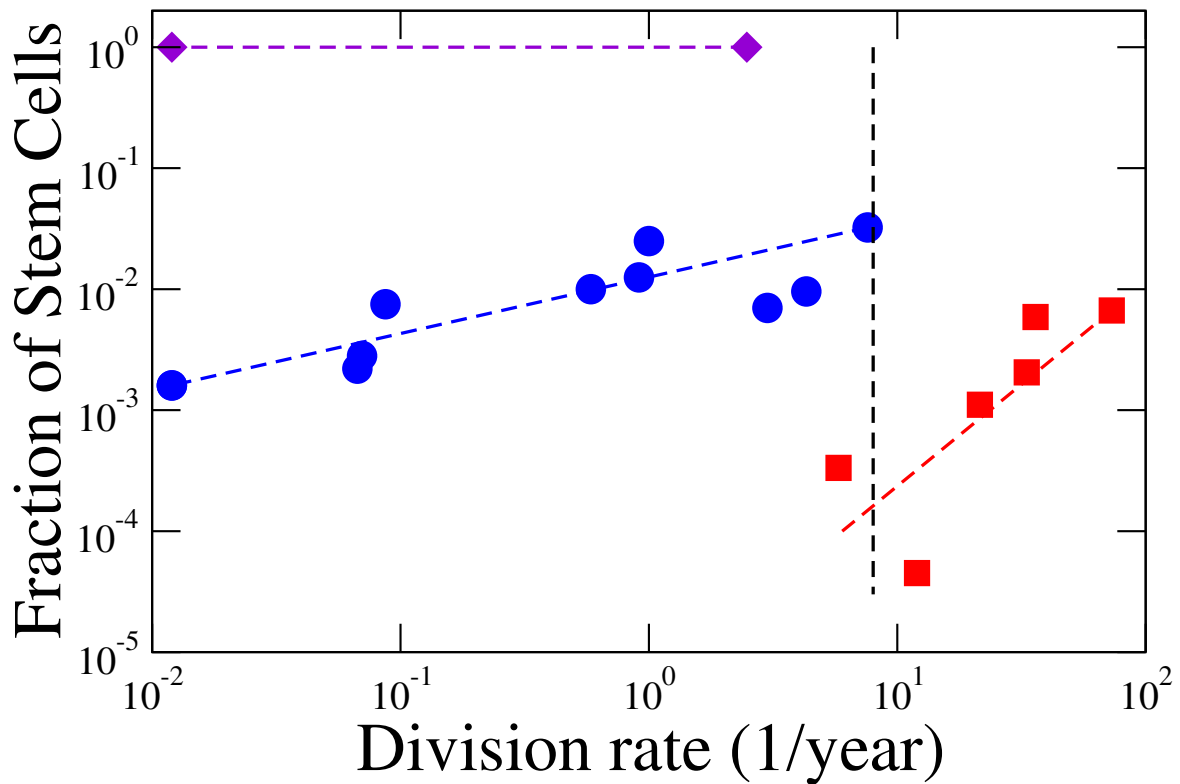
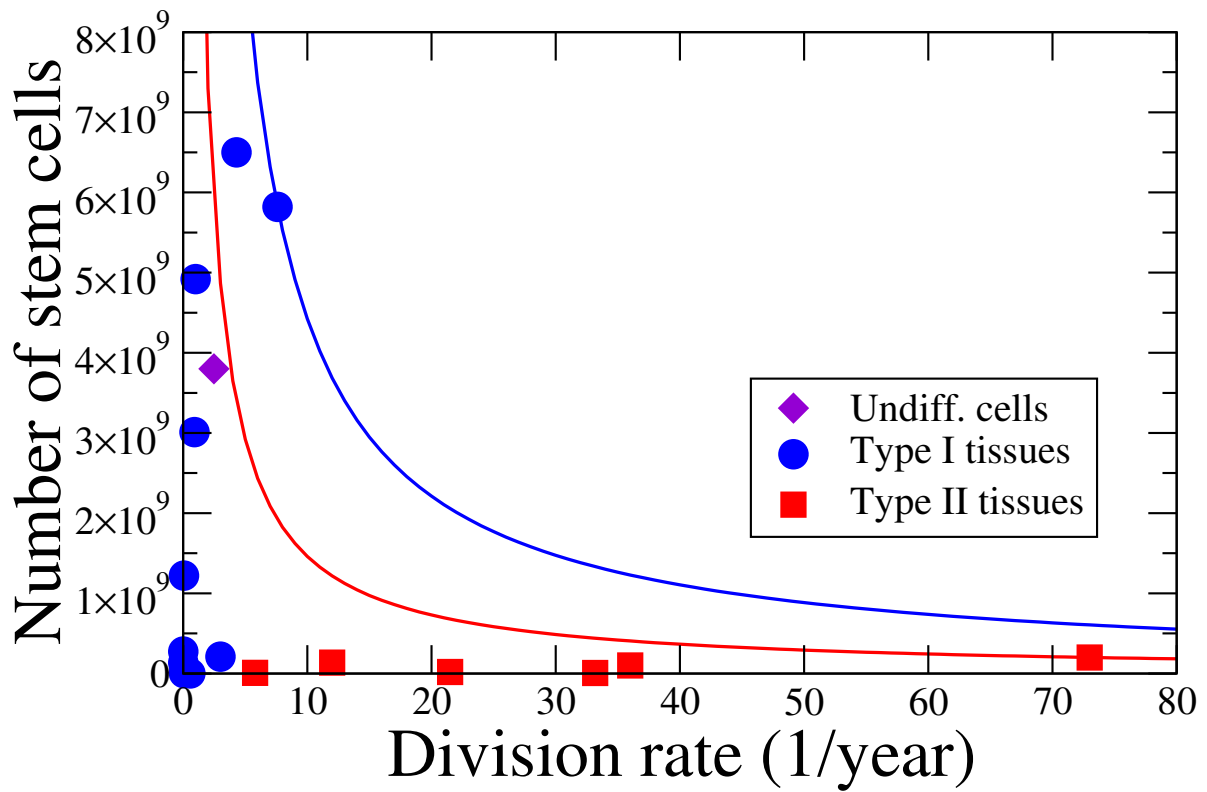


**Figure 2.** Top: Representation of tissues from Table 1 as points in the  $(m_s, N_s)$  plane. Hyperbolae containing the colon (red) and the epidermis (blue) are drawn as illustrations. Bottom: A log-log plot of  $N_s/N_{cell}$  vs  $m_s$ , where tissue clustering becomes more apparent. Dashed lines are guides to the eyes. The vertical one corresponds to  $m_s = 8$ /year.

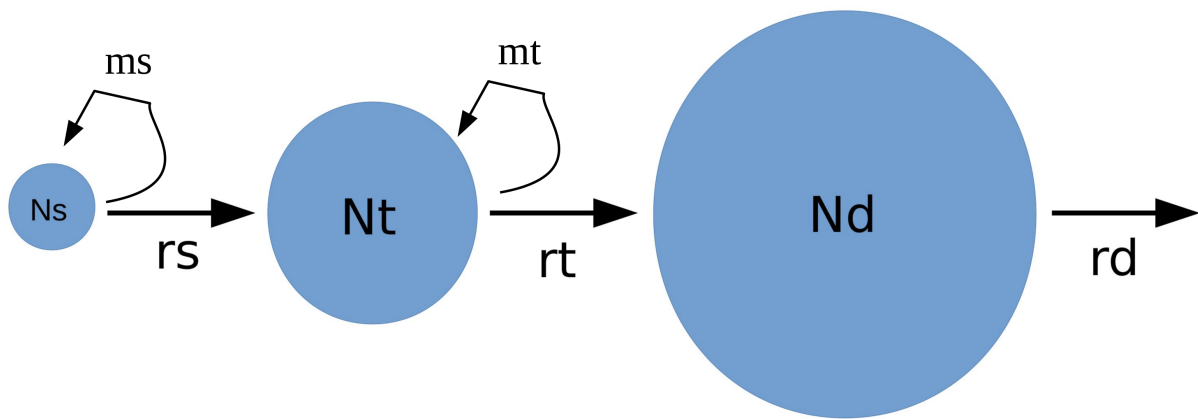


**Figure 3.** Schematic representation of homeostasis in a tissue. See explanation in the main text.